Author Manuscript

Using Space-Based CO_2 and NO_2 Observations to Estimate Urban CO_2 Emissions

Emily G. Yang[1], Eric A. Kort[1], Lesley E. Ott[2], Tomohiro Oda[3,4,5], and John C. Lin[6]

[1]Department of Climate and Space Sciences and Engineering, University of Michigan, Ann Arbor, MI 48109, USA, [2]Global Modeling and Assimilation Office, NASA Goddard Space Flight Center, Greenbelt, MD 20706, USA, [3]Earth from Space Institute, Universities Space Research Association (USRA), Columbia, MD 21046, USA, [4]Department of Atmospheric and Oceanic Science, University of Maryland, College Park, MD 20742, USA, [5]Graduate School of Engineering, Osaka University, Suita, Osaka 565-0871, Japan, [6]Department of Atmospheric Sciences, University of Utah, Salt Lake City, UT 84132, USA

Corresponding author: Emily G. Yang (egyang@umich.edu)

Key Points:

- We use empirical relationships between satellite observations of CO_2 and NO_2 to generate NO_2-derived CO_2 fields to estimate CO_2 emissions.
- We demonstrate NO_2-derived CO_2 emissions estimates on a monthly scale that are comparable to monthly emissions inventory estimates.
- Wide availability of NO_2 data drastically reduces NO_2-derived CO_2 emissions estimate uncertainties when aggregated over a month or more.

This is the author manuscript accepted for publication and has undergone full peer review but has not been through the copyediting, typesetting, pagination and proofreading process, which may lead to differences between this version and the Version of Record. Please cite this article as doi: 10.1029/2022JD037736.

This article is protected by copyright. All rights reserved.

Author Manuscript

Abstract

As the majority of fossil fuel carbon dioxide (CO_2) emissions originate from cities, the use of novel techniques to leverage available satellite observations of CO_2 and proxy species to constrain urban CO_2 is of great importance. In this study, we seek to empirically determine relationships between satellite observations of CO_2 and the proxy species nitrogen dioxide (NO_2), applying these relationships to NO_2 fields to generate NO_2-derived CO_2 fields (NDCFs) from which CO_2 emissions can be estimated. We first establish this method using simulations of CO_2 and NO_2 for the cities of Buenos Aires, Melbourne, and Mexico City, finding that the method is viable throughout the year. For the same three cities, we next calculate empirical relationships (slopes) between co-located observations of NO_2 from the Tropospheric Monitoring Instrument (TROPOMI) and Snapshot Area Mode (SAM) observations of CO_2 from Orbiting Carbon Observatory-3 (OCO-3). Applying varying combinations of slopes to generate NDCFs, we evaluate methodological uncertainties for each slope application method and use a simple mass balance method to estimate CO_2 emissions from NDCFs. We demonstrate monthly urban CO_2 emissions estimates that are comparable to emissions inventory estimates. We additionally prove the utility of our method by demonstrating how large uncertainties at a grid cell level (equivalent to ~1-3 ppm) can be reduced substantially when aggregating emissions estimates from NDCFs generated from all NO_2 swaths (about 1-6%). Rather than rely on prior knowledge of emission ratios, our method circumvents such assumptions and provides a valuable observational constraint on urban CO_2 emissions.

Plain Language Summary

We can improve our understanding of urban fossil fuel carbon dioxide (CO_2) emissions by observing gases that are emitted simultaneously with CO_2 when fossil fuels are burned, like nitrogen dioxide (NO_2). Here, we develop a method to enhance our understanding of urban CO_2 emissions by using relationships between CO_2 and NO_2, with observations from satellites. In this method, we find relationships between CO_2 and NO_2 when we have observations of both, and then apply these relationships to NO_2 observations lacking corresponding CO_2 observations, thereby generating NO_2-derived CO_2 fields. We can then estimate CO_2 emissions from these NO_2-derived CO_2 fields without any prior assumption of emission ratios of these gases. We first test the method using simulations of these gases for the cities of Buenos Aires, Melbourne, and Mexico City. We then apply the method to space-based observations of CO_2 for the same cities. CO_2 emissions estimated from the observation-based NO_2-derived CO_2 fields demonstrate monthly variations that have previously not been demonstrated using satellite observations. Leveraging the larger quantity of available NO_2 observations allows us to derive emissions estimates with greater precision when we aggregate the estimates over periods of a month or greater.

1 Introduction

As the global carbon dioxide (CO_2) mixing ratio rises, the importance of assessing fossil CO_2 emissions from cities is magnified. At present, the majority of fossil CO_2 emissions entering the atmosphere originate from urban areas, resulting mostly from automobile tailpipe emissions, industrial emissions, home heating, and fossil fuel-based power plants, though the lattermost emissions often take place away from the urban center itself (International Energy Agency, 2008; Lin et al., 2018). As of 2018, 55% of the global population resided in urban areas, and this proportion is projected to increase to 68% by 2050 (United Nations, Department of Economic

This article is protected by copyright. All rights reserved.

and Social Affairs, Population Division, 2019). Not only are urban fossil CO_2 emissions expected to play an increasingly important role in the global carbon cycle, but also their quantification is becoming a higher priority as cities pledge to reduce emissions (Bodansky, 2016; Gurney et al., 2015; Rosenzweig et al., 2010) and require a means of assessing progress toward pledged goals (Lauvaux et al., 2020; Mueller et al., 2021). However, there are many gaps in our understanding of urban carbon emissions, along with high uncertainties, due in large part to limited data collected at the urban scale (Gately & Hutyra, 2017; Hutyra et al., 2014). In more recent years, there has been a push to fill this gap using space-based observations of CO_2 to better understand urban emissions (Kort et al., 2012; Hakkarainen et al., 2016; Hedelius et al., 2018; Wu et al., 2018; C. Park et al., 2020; Wu et al., 2020; Yang et al., 2020; Ye et al., 2020; Kiel et al., 2021; H. Park et al., 2021; Lei et al., 2021, 2022; Kuze et al., 2022). However, space-based observations of urban CO_2 are also limited, as current satellites like the Greenhouse gases Observing SATellite (GOSAT) and Orbiting Carbon Observatory-2 (OCO-2) were designed to focus on spatiotemporal distribution of biospheric carbon fluxes on regional scales, rather than to quantify anthropogenic emissions (Nassar et al., 2017).

Observation of gaseous species that are co-emitted with fossil CO_2 during combustion has the potential to provide much-needed information to fill the urban carbon cycle knowledge gaps. These proxy species, such as the nitrogen oxides family (NO_x) and carbon monoxide (CO), share many sources that are co-located in time and space with those of CO_2, and thus can be used to help constrain fossil CO_2 emissions and monitor temporal changes in emissions (Berezin et al., 2013; Konovalov et al., 2016). In particular, observations of nitrogen dioxide (NO_2), one of the gases in the NO_x family, have the potential to greatly increase our understanding of urban carbon emissions for a variety of reasons. Using NO_2 as a proxy for fossil CO_2 allows for the quantification of anthropogenic emissions and disentanglement from biogenic sources of CO_2 (Ciais et al., 2014; Goldberg et al., 2019). Additionally, the relatively short lifetime of NO_2 means that observed NO_2 concentrations are less affected by long-range transport than CO_2 or longer-lived proxies like CO, and lend themselves to more robust interpretation in a local setting (Berezin et al., 2013; Goldberg et al., 2019). For example, the shorter lifetime of NO_2 allowed Fujinawa et al. (2021) to estimate CO_2 emissions from power plants using concurrent airborne observations of both CO_2 and NO_2 in an urban area in Japan, with the NO_2 plumes providing constraints to the CO_2 plumes. NO_2 observations are also less sensitive to clouds than those of CO_2, and quantification of NO_2 emissions is less affected by background variability (Kuhlmann et al., 2019).

Space-based NO_2 observations in particular have the potential to improve the quantification of CO_2 emissions. Satellite observations of NO_2 have been used in combination with NO_x:CO_2 inventory ratios to indirectly estimate CO_2 emissions. For example, Berezin et al. (2013) used NO_2 observations from the Global Ozone Monitoring Experiment (GOME) and the SCanning Imaging Absorption spectroMeter for Atmospheric CHartographY (SCIAMACHY) space-based instruments to infer NO_x emissions, then used NO_x:CO_2 emission conversion factors defined by the Emission Database for Global Atmospheric Research (EDGAR) and the Regional Emission Inventory in Asia (REAS) to estimate multiannual trends of CO_2 emissions in China. Konovalov et al. (2016) also made regional estimates of CO_2 emissions in Western Europe using satellite observations of both proxy species NO_2 and CO from the Ozone Monitoring Instrument (OMI) and the Infrared Atmospheric Sounding Interferometer (IASI) in combination with EDGAR emission ratios, finding that NO_2 observations had the potential to provide much stronger constraints to the total annual fossil CO_2 emissions in the study region than those of CO.

This article is protected by copyright. All rights reserved.

Author Manuscript

More recent studies have used similar methods to constrain CO_2 emissions at smaller scales, with Goldberg et al. (2019) using OMI NO_2 observations and NO_x:CO_2 ratios from the U.S. EPA to infer CO_2 emissions from eight U.S. megacities, while Liu et al. (2020) indirectly estimated CO_2 emissions from eight U.S. power plants by combining OMI NO_2 observations with the NO_x:CO_2 relationship reported by continuous emissions monitoring system (CEMS) programs. There are limitations to studies that rely on prior NO_x:CO_2 ratios, however, as such studies are dependent on the accuracy and timeliness of the reported ratios and often the assumption that observed atmospheric enhancement ratios match emission ratios. While they could not directly obtain uncertainties on this ratio for their study region, Konovalov et al. (2016) estimated it by finding differences in the ratio across three emissions inventories, ranging from 1.4 to 24.9%. The NO_x:CO_2 relationship can also change with time, whether seasonally or interannually as a result of changes in emissions capturing technology, shifting energy production and transport patterns, or other factors. The temporal offset between updates in emissions inventories, often lasting a year or more, would hinder near-real-time studies relying on up-to-date ratios.

There have also been studies that have leveraged satellite NO_2 observations to provide additional information to existing satellite CO_2 observations. In this vein, Reuter et al. (2019) used NO_2 observations from the TROPOspheric Monitoring Instrument (TROPOMI) to adjust wind direction and constrain the shape of the CO_2 plume observed by the OCO-2 to make CO_2 flux estimates for six case studies of various cities, power plants, and wildfires. Kiel et al. (2021) also related CO_2 observations of Los Angeles from the Orbiting Carbon Observatory-3 (OCO-3) instrument to TROPOMI NO_2 observations to ensure that the observed CO_2 distributions showed true signals derived from local emissions. Finally, Hakkarainen et al. (2021) derived a mean NO_x:CO_2 ratio from co-located TROPOMI and OCO-2 observations of the Matimba power plant in South Africa, then applied the ratio to annual NO_x emissions derived from TROPOMI to make CO_2 flux estimates that were consistent with Open-source Data Inventory for Anthropogenic CO_2 (ODIAC) estimates.

In this study, we demonstrate a method for estimating urban CO_2 emissions using NO_2-derived CO_2 fields (NDCFs) empirically derived from space-based observations of urban CO_2 and NO_2, and we assess this method using simulated and observational data for the cities of Buenos Aires, Melbourne, and Mexico City. Rather than relying on prior knowledge of NO_x:CO_2 emission ratios, as did Berezin et al. (2013), Konovalov et al. (2016), Goldberg et al. (2019), and Liu et al. (2020), our method circumvents such assumptions and depends instead on finding empirical relationships between observations of column-averaged dry-air mole fraction of CO_2 (XCO_2) from OCO-3 and tropospheric NO_2 observations from TROPOMI. These relationships can then be applied to TROPOMI NO_2 data to generate NDCFs for time periods that have no co-located CO_2 observations. Inverse methods can then be used on the NO_2-derived CO_2 fields to estimate CO_2 emissions. We evaluate the feasibility of this method using co-located Goddard Earth Observing System Composition Forecast (GEOS-CF) simulations of XCO_2 and NO_2, and we demonstrate the method with observations from OCO-3 and TROPOMI. We further assess mass balance estimates of CO_2 emissions based on the NDCFs, and discuss uncertainties associated with this method. Given the relative abundance and resolution of space-based NO_2 observations compared to those of CO_2, we explore the potential our method has on the constraint of urban CO_2 emissions, highlighting the utility of our method in generating urban emissions estimates at an unprecedented temporal scale that have not yet been achieved by satellite observations.

This article is protected by copyright. All rights reserved.

Author Manuscript

2 Data and Methods

The goal of this study is to demonstrate a method of generating urban NO_2-derived CO_2 fields (NDCFs) from empirical relationships between observations of CO_2 and NO_2, and use these NDCFs to estimate emissions of CO_2. We first establish this method using simulations of these gases, as our pool of available observations is limited. We then find empirical relationships from available co-located satellite observations of CO_2 and NO_2 to explore the utility of the method and emissions estimates based on the method. Our areas of focus are the following three cities: Buenos Aires, Argentina (34.6037° S, 58.3816° W); Melbourne, Australia (37.8136° S, 144.9631° E); and Mexico City, Mexico (19.4326° N, 99.1332° W). We study these three cities due to availability and quality of SAM observations at the time of the beginning of the study, as well as because these cities are located throughout the world in different countries, with varying topography and emissions characteristics.

2.1 Simulation Data and Methods

2.1.1 Simulation Data and Pre-Processing

We use hourly simulations of CO_2 and NO_2 from the GEOS-CF system focused on our cities of interest (Keller et al., 2021; GEOS-CF., 2022). The GEOS-CF system is a 0.25° global constituent prediction system that combines the GEOS weather and aerosol modeling system with the GEOS-Chem chemistry module, simulating various atmospheric constituents such as CO_2 and NO_2 in the past, as well as five-day forecasts of said constituents. The CO_2 surface fluxes are described by Weir et al. (2021) and are derived from multiple sources, including the Open-Data Inventory for Anthropogenic Carbon dioxide (ODIAC) for fossil fuel emissions (Oda & Maksyutov 2015; Oda et al., 2018). The primary source of anthropogenic NO_x fluxes used in the GEOS-CF system is the Hemispheric Transport of Air Pollution emissions inventory (Janssens-Maenhout et al., 2015). The chemical mechanisms involved in simulating NO_x are described in detail by Keller et al. (2021) and include gas-phase processes such as photolysis.

For this study, we use concurrent and co-located hourly CO_2 (dry air column-averaged mixing ratio) and tropospheric column NO_2 (tropospheric vertical column density) simulations for our three cities of interest. We use data from each season, with one week's worth of data in April(2019-04-14 to 2019-04-20), July (2019-07-14 to 2019-07-20), and October (2019-10-13 to 2019-10-19), and four weeks' worth of data in January and February (2020-01-12 to 2020-02-08). Note that there are a few gaps in the January and February CO_2 data, with six hourly simulations missing from the first week and one missing from each of the following weeks. Figure 1a and b show an example of a set of co-located CO_2 and NO_2 simulations for Buenos Aires in April 2019.

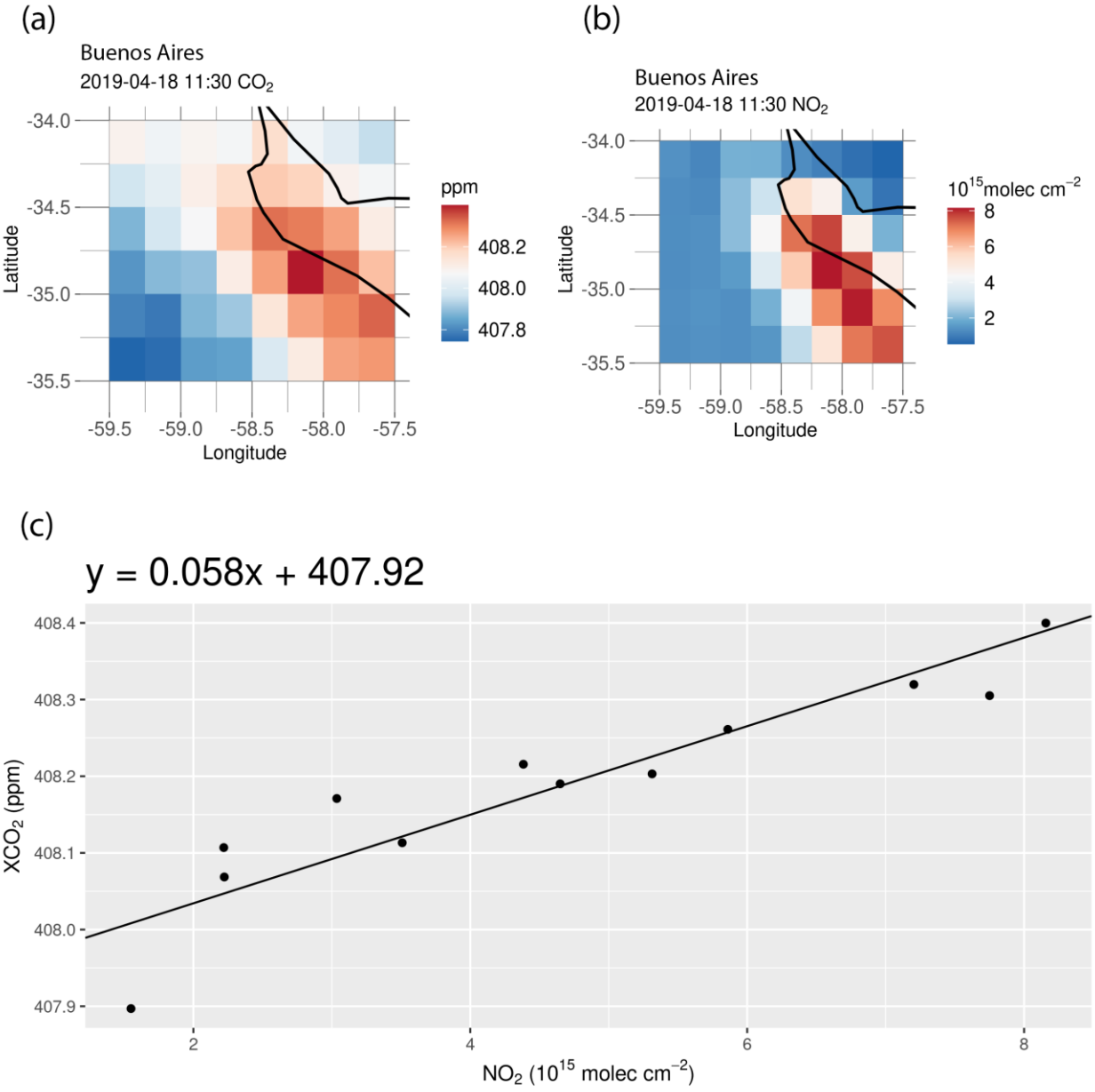
We choose separate domains of interest for each city of interest, focusing on the area emitting CO_2 with the highest intensity. These domains are chosen by comparing the spatial boundaries of the cities shown on Google Earth with the areas of highest carbon emission represented by ODIAC (Oda et al., 2018). The domain for Buenos Aires is 1.0° × 0.75° in size, and the domains for Melbourne and Mexico City are both 0.75° × 0.75° squares.

Once domains are chosen, we filter the simulations. We only use hours during which daylight is present for each location. Additionally, we filter out co-located sets of simulations with the highest 95th percentile of NO_2 values greater than 1.5×10^{16} molecules cm^{-2}. The presence of high NO_2 values is indicative of stagnation events, which affect the CO_2-NO_2

This article is protected by copyright. All rights reserved.

Author Manuscript

relationship and result in calculation of slopes that are not representative. As such, we exclude simulations with these high values. We then calculate the CO_2-NO_2 slopes and intercepts for daytime simulations (see Figure 1c) and filter for Kendall rank correlation coefficient (at least 0.1), R^2 (at least 0.1), and slope (must be positive). The simulations are further screened via visual inspection to ensure clarity of plumes.



This article is protected by copyright. All rights reserved.

Figure 1. An example of a set of hourly, co-located GEOS-CF simulations of (a) CO_2 and (b) NO_2, and (c) the relationship between the two, in April 2019 in Buenos Aires ($R^2 = 0.85$).

2.1.2 Simulating NO_2-Derived CO_2 Fields, Evaluating Simulated Uncertainties, and Assessing Sensitivity to Seasonal Changes

To generate NDCFs, we multiply single slopes with an NO_2 field from an hour different from which the slopes are derived. The field generated in such a manner represents an NO_2-derived CO_2 enhancement field. When the intercept associated with the slope is added to the enhancements, the resulting field is an NO_2-derived CO_2 concentration field. Note that these NDCFs represent total CO_2, with the empirical slopes capturing all impacts from the biosphere or chemistry.

To estimate uncertainties from the simulations, we group simulations by city and season, and we generate concentration fields by applying each calculated slope and intercept in a season to every other NO_2 simulation in that season. Next, we find the relative difference between the individual grid values of the NDCFs and those of the "true" CO_2 fields that temporally correspond to the NO_2 fields from which the NDCFs are derived. The standard deviation (σ) of the gridded relative differences serves as a measure of the uncertainty of each simulated NDCF grid cell.

We test the sensitivity of the NDCFs to seasonal changes in biosphere activity and NO_2 chemical lifetime by assessing the seasonality of the uncertainties.

2.2 Observation Data and Methods

2.2.1 Satellite Data and Pre-processing

For our CO_2 observations (dry air column-averaged mixing ratio), we use bias-corrected OCO-3 Level 2 Lite, version 10.4r data in Snapshot Area Map (SAM) mode (Eldering et al., 2019; OCO-2/OCO-3 Science Team et al., 2022). These SAMs are fine-scale spatial samplings (with footprint size of 4 km^2 or smaller) of large contiguous areas (~80km × 80km) that generally target urban centers, and the overpass times are variable. We filter the SAMs so that they have at least 1000 soundings each, with reasonable data density near the city center of interest, and all adopted data points are screened by quality flag. Additionally, in the two cases found when the CO_2 field demonstrates enhancements on the edge of a SAM far from and unrelated to the urban center, the enhanced edge is masked out.

For our NO_2 observations, we use Level 2 version 1 observations of tropospheric NO_2 tropospheric vertical column density (with resolution of 5.5 km × 3.5 km) from the TROPOMI instrument onboard the Sentinel-5P satellite, which has an overpass time of about 13:30 local solar time and a swath width of ~2600 km (Copernicus Sentinel-5P, 2018; Veefkind et al., 2012). We define the "source area domain" as the same domains used in the GEOS-CF simulations (Section 2.1.1). We define the "surrounding domain" as a larger area surrounding the source area domain, generally an additional 0.5° box around. The TROPOMI swaths are filtered similarly to those used by Huber et al. (2020), as follows. Only pixels with "flag_value" greater than or equal to 0.75 are used. Next, we only use swaths with at least 30 pixels in the source area domain and 30 pixels in the surrounding domain. Finally, the number of passing pixels must be at least 25% the total number of pre-filtered pixels. As with the GEOS-CF simulations, we also filter out

This article is protected by copyright. All rights reserved.

Author Manuscript

swaths whose highest 95th percentile of NO_2 values are greater than 1.5×10^{16} molecules cm^{-2} so as to exclude observations that indicate stagnation events (~2% of available TROPOMI swaths).

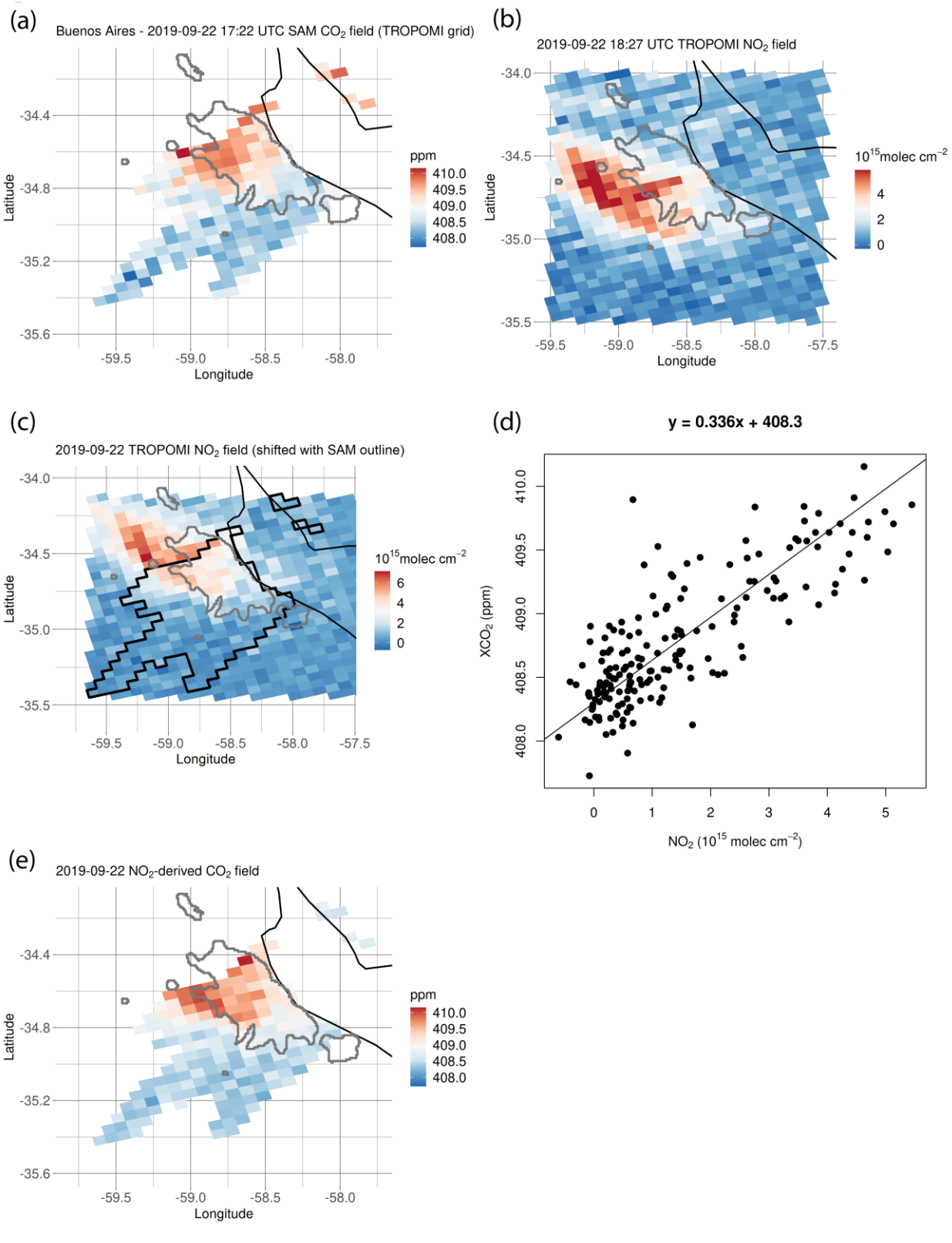
As an additional filter, we plot co-located SAMs and TROPOMI swaths and visually inspect them to ensure plume clarity. We use available SAMs and TROPOMI swaths from the end of 2019 through mid-2021. For Buenos Aires, the dates span from 2019-09-18 to 2021-05-27. For Melbourne, the dates span from 2020-01-13 to 2021-07-01. For Mexico City, the dates span from 2020-02-08 to 2021-06-21.

2.2.2 Defining Empirical Relationships between CO_2 and NO_2 Observations and Generating NDCFs

As with the GEOS-CF simulations, we calculate slopes and intercepts between co-located and semi-concurrent observations. Figure 2 shows an example of this process. Because the satellites pass over the cities of interest at different times, we must account for the time difference. We spatially shift the NO_2 field by increments of 0.01° in each direction up to 0.3° and calculate the Kendall rank correlation coefficient after each shift between the CO_2 values, which are averaged to fit the corresponding TROPOMI grid, and the NO_2 values, which are spatially masked to match the outline of the SAM. If the highest correlation coefficient found is less than 0.2, that co-located set of observations is filtered out. Otherwise, the shift corresponding to the highest correlation coefficient is then applied to the NO_2 field, and the slope and intercept are calculated using a ranged major axis regression. Additionally, co-located sets can be filtered out through visual inspection if there are no clear plumes.

Author Manuscript

This article is protected by copyright. All rights reserved.



This article is protected by copyright. All rights reserved.

Figure 2. (a) An example of a SAM in Buenos Aires. The values have been averaged to match the corresponding TROPOMI grid. The gray line outlines the area of the highest 90th percentile of CO_2 emissions values in the area from ODIAC, which roughly corresponds to the urban area. The thin black line shows country borders. (b) The corresponding TROPOMI NO_2 field from the same day, observed about one hour after the SAM. (c) The same NO_2 field shifted spatially to have the highest correlation with the CO_2 data and masked to match the SAM, whose shape is outlined in the thick black line. (d) Scatterplot of CO_2 and NO_2 data from plots (a) and (c) from which the empirical relationship can be found. The R^2 value for the linear regression is R^2 = 0.66. (e) NDCF generated using relationship from (d) applied to the field in (c).

Once the empirical relationships have been found between the co-located CO_2 and NO_2 fields, NDCFs can be generated. We generate NDCFs from NO_2 swaths that have corresponding SAMs (e.g., Figure 2e), and we also generate NDCFs from the large quantity of NO_2 swaths that do not have corresponding SAMs. For when we have co-located observations, we use a circular application of slopes, i.e., we apply the same-day slopes and intercepts to the NO_2 field to make direct comparisons with the corresponding SAM. For the non-co-located NDCFs, we apply slopes and intercepts with the following four different methods. 1) Single Slope: one slope at a time is applied to all NO_2 fields temporally following a set of co-located observations until the next co-location occurs. This is a simple method that can be used in near-real-time, as opposed to a method that would use the slope from the temporally closest co-location, which would require post hoc information. 2) Average Slope: all available slopes are averaged together and applied to every NO_2 field. 3) Single Slope with Baseline: similar to the single slope method, but each slope is also averaged with the average slope value, to capture temporal variations but dampen noise. 4) Rolling Averages: averages of multiple slopes are applied to subsequent NO_2 fields, in a similar fashion to the Single Slope method but with several slopes averaged together. For Buenos Aires and Mexico City, we use rolling averages of two, three, four, and five slopes, out of a total of 12 slopes for both these cities. For Melbourne, we only use a rolling average of two slopes, as the number of Melbourne SAMs that pass our filters, and thus number of slopes available to us, is only three.

2.2.3 Estimating CO_2 Emissions with a Simple Mass Balance Method

To estimate CO_2 emissions, we use a simple mass balance method similar to that described by Buchwitz et al. (2017). In their study, Buchwitz et al. demonstrated a fast method of emissions estimation for time-averaged satellite observations of methane. We apply their method to SAMs and NDCFs with a few changes to account for the different application. Note that we use this emissions estimate method to be able to fairly quickly generate a large quantity of order-of-magnitude emissions estimates with some temporal variations rather than precise emissions estimates; this mass balance method is not a part of the NDCF method we are describing in this study.

The mass balance method is based on a box model, in which the "box" described is the CO_2 source region, e.g., the domain of the city of interest. The emissions E associated with the source region are given as

$$E = CF \times \Delta C \times V/L, \quad (1)$$

where CF is a correction factor, ΔC is the average enhancement in the source region as a vertical column density, V is the wind speed, and L is the length of the box. Regarding CF and V,

This article is protected by copyright. All rights reserved.

Buchwitz et al. used $CF = 2$ and a constant V of 1.1 m s^{-1}, which were derived by calibrating their estimates to the Copernicus Atmosphere Monitoring Service (CAMS) inventory. As we are not using time-averaged observations, we use 10 m wind speeds from the ERA5 reanalysis data (Hersbach et al., 2018; Hersbach et al., 2020), averaging the wind speeds over the domain. With wind speeds of approximately 3-6 m s^{-1}, we also calibrate to inventory data and find that $CF = 1/3$ is sensible for our study, which results in a combined CF × V value that is fairly comparable to that used by Buchwitz et al. For ΔC, we first find the average concentration in the source region and subtract off a background value, which we determine to be the average value of the lowest 20th percentile of values within the bounds of the surrounding domain. We then convert this enhancement from units of ppm to kg m^{-2} using a simple conversion factor of 0.01 kg m^{-2} per 1 ppm of enhancement, as described by Kuhlmann et al. (2020). Regarding L, we use an average of the ERA5 wind direction in the source region to determine whether the winds are flowing in a more north-south direction or east-west direction. Depending on this direction, we use the corresponding length of the domain as L. Note that the magnitude of the emissions estimates derived from this mass balance method depend heavily on how CF or V are calibrated to a prior, which is a weakness of the method; we use this method for its speed in calculating large numbers of estimates but recommend more robust methods of emissions estimation when more precise estimates are desired.

We use the mass balance method to estimate CO_2 emissions from SAMs, corresponding co-located NDCFs, and NDCFs generated with the four slope application methods described in Section 2.2.2. We also make comparisons between our emissions estimates and EDGAR v5.0 monthly sector-specific gridmaps of CO_2 emissions for the year 2015 (Crippa et al., 2019; Crippa et al., 2020), summing the inventory emissions from the same source area domains of the cities as those used in the mass balance estimates. We combine emissions from the four sectors that produce the most emissions in cities: power industry, manufacturing, road transport, and buildings. Note that the only monthly-scale EDGAR gridmaps that are publicly available are sector-specific. As described by Crippa et al. (2020), the hourly, daily, and monthly temporal profiles used to produce these gridmaps were generated by grouping regions of the world by climate zones, heating degree days (a measure of how weather affects energy demand), and ecological zones, and then the profiles were matched to each EDGAR process (e.g., energy, industry, and residential, with 227 total processes) and each country to then disaggregate annual emissions by sector and month.

2.2.4 Evaluating Methodological Uncertainties

Following a process similar to that used to determine simulation uncertainties in Section 2.1.2, we here use the spread of relative differences in the observational data to estimate methodological uncertainties, capturing the uncertainties associated with the slope calculations and with the assumptions behind the method itself. Grouping the co-located data by city, we generate separate sets of NDCFs by applying our four slope application methods to every NO_2 field in the group, with the exception of fields whose slopes were used in the slope calculation. Specifically for the Average Slope method, we find an average of every slope except one and apply the average to that corresponding NO_2 field, and rotate through all available co-located datasets. Once the separate sets of NDCFs are generated, we again calculate the standard deviation of relative differences of individual grid cells between SAMs and the corresponding NDCFs generated with the different methods. These standard deviations serve as a measure of the methodological uncertainty that can be propagated through to NDCF emissions estimates.

This article is protected by copyright. All rights reserved.

Author Manuscript

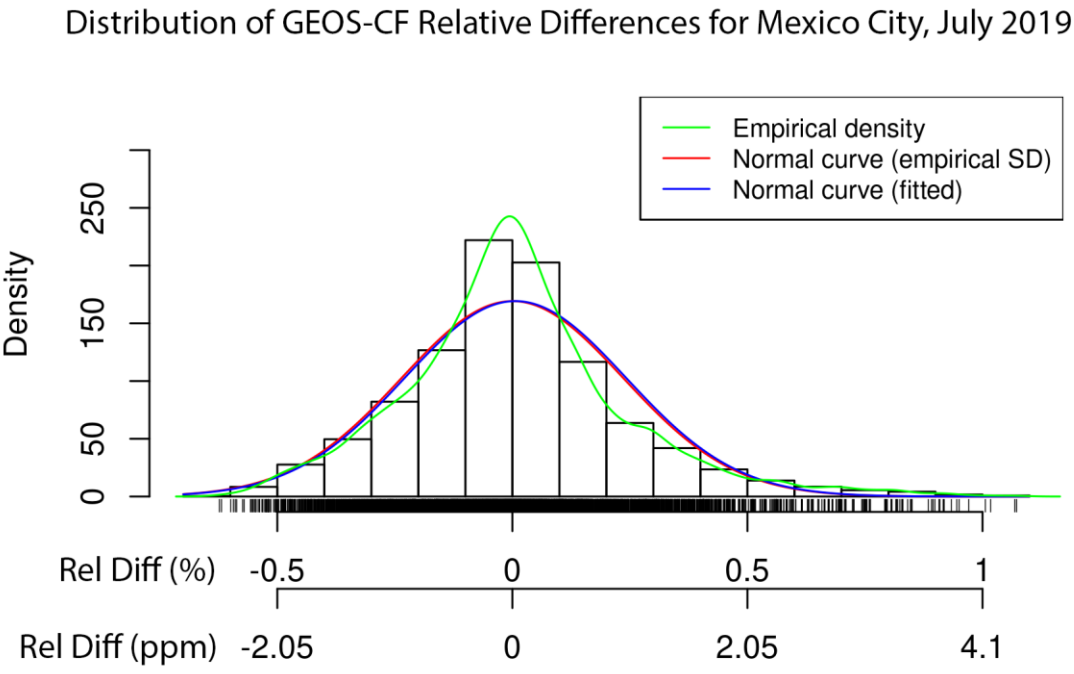
The methodological uncertainty is derived relative to concentration, as opposed to enhancement, in order to ensure that there is some uncertainty regardless of the level of enhancement.

Note that we do not include an evaluation of uncertainties from the mass balance method. This study assesses the utility of the NDCF method and not the mass balance method, and uncertainties associated with the mass balance method would be large enough to mask the effect of the NDCFs on their own.

3 Results

3.1 Establishment of the NDCF Method with GEOS-CF Simulations and Co-located Observations

Generating simulation-based NDCFs with reasonable levels of error and low bias in comparison to the "true" CO_2 simulations suggests that the NDCF method can be reasonably applied to observations. Following the methods described in Section 2.1.2, we generate simulation-based NDCFs with application of a single slope for each city and season, find the relative differences between the NDCFs and their "true" counterparts, and use the spread of the distribution of these relative differences at grid cell-level as a measure of the simulation-based uncertainty. An example distribution of the relative differences for Mexico City (July) is found in Figure 3. For this example, the standard deviation of the relative differences is 0.24% of the total concentration of a grid cell, which is equivalent to 0.97 ppm if we assume a concentration of 410 ppm to illustrate order-of-magnitude uncertainties in units of ppm. There is low bias associated with this example because the Gaussian distribution corresponding to the standard deviation of the data and the Gaussian distribution fit to the data are almost the same. This is the same for all other seasons and cities as well.



This article is protected by copyright. All rights reserved.

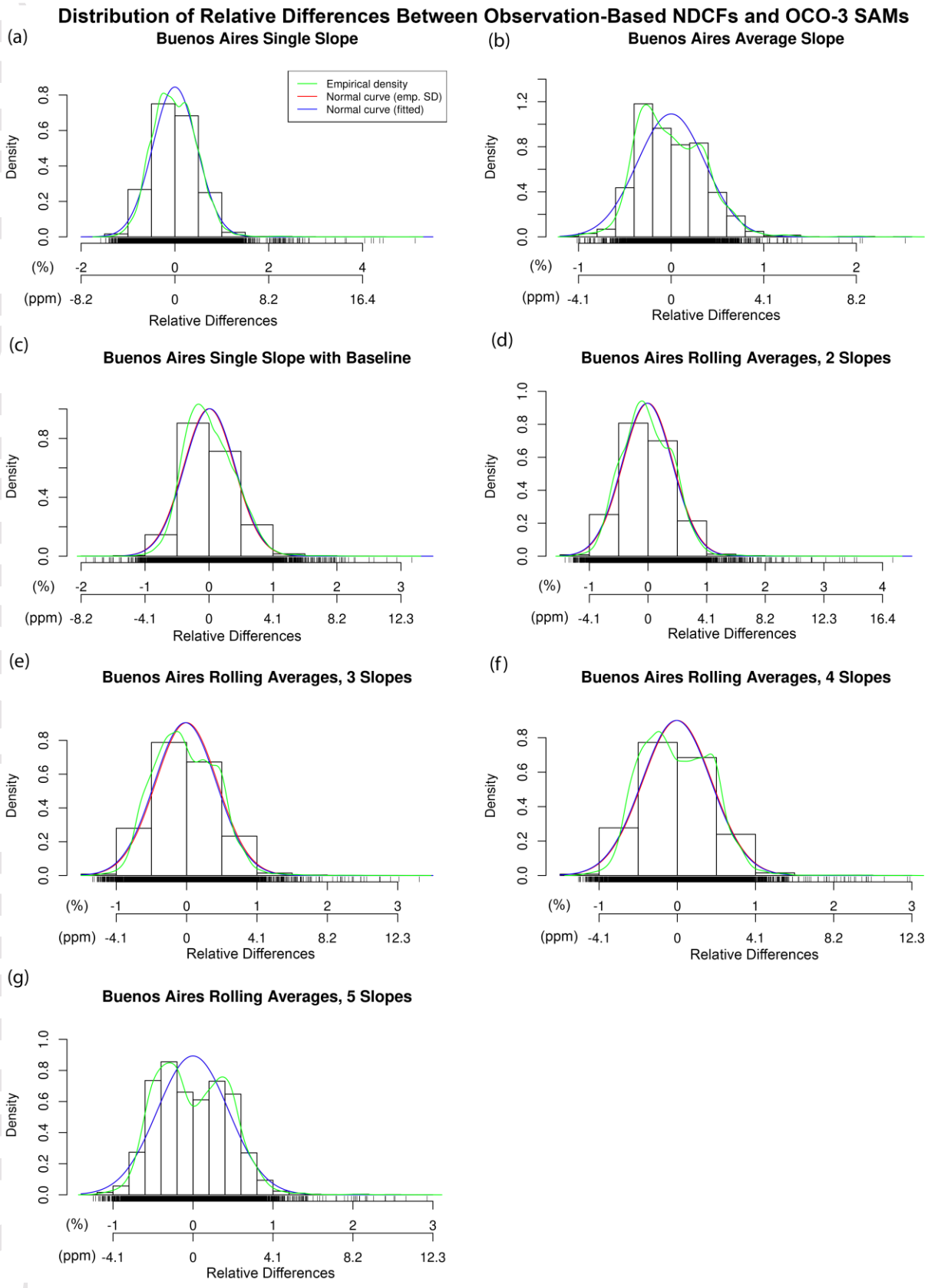
Figure 3. An example of the simulation-based distribution of grid cell-level relative differences between NDCF and "true" counterparts, for Mexico City July 2019 (summer). The green line shows the empirical density curve, the red line shows the Gaussian curve using the standard deviation of the relative differences, and the blue curve fits a Gaussian to the data. Because the red and blue curves are very similar to each other, there is low bias. The standard deviation of the relative differences for this example is 0.24% of the total concentration of a grid cell, which would be equivalent to 0.97 ppm if we assume a concentration of 410 ppm as an example value for illustrative purposes.

We also use mass balance CO_2 emissions estimates from co-located observations for all three cities to demonstrate the viability of the NDCF method in combination with a simple method of emissions estimation. Figure S1 shows mass balance estimates of SAMs for the three cities, as well as estimates of corresponding NDCFs derived from circular slope application. A comparison between SAM and NDCF emissions estimates shows them to be within the same order of magnitude, and many of the dates presented in Buenos Aires are quite similar to each other (Figure S1a). However, we do also expect differences due to the methodological uncertainties, as well as uncertainties due to the mass balance method itself. Estimates of NDCF emissions being in the same order of magnitude as SAM emissions is a reasonable demonstration of effectiveness given the large uncertainties expected.

Author Manuscript

This article is protected by copyright. All rights reserved.

Author Manuscript



This article is protected by copyright. All rights reserved.

Figure 4. Distributions of relative differences, as in Figure 3, but for Buenos Aires observation-based NDCFs derived using the different slope application methods generated using 12 sets of observations: (a) Single Slope, (b) Average Slope, (c) Single Slope with Baseline, (d) Rolling Averages (two slopes), (e) Rolling Averages (three slopes), (f) Rolling Averages (four slopes),

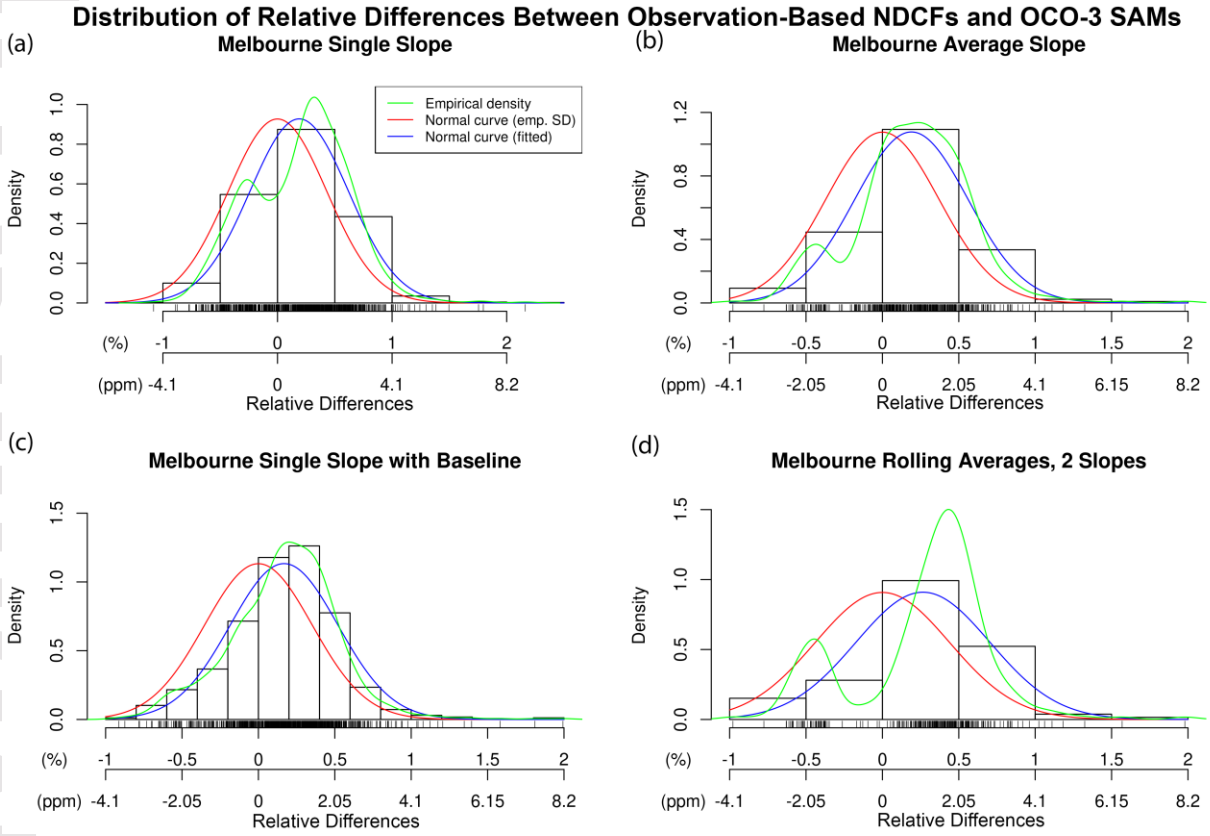


Figure 5. Same subplots as Figure 4 (a-d), but for Melbourne, generated using three sets of observations. Note that the low number of SAM observations limits the Rolling Averages method to two slopes only.

	Buenos Aires	*Melbourne*	*Mexico City*
Single Slope	0.47% (1.94 ppm)	0.43% (1.76 ppm)	0.79% (3.26 ppm)
Average Slopes	0.37% (1.50 ppm)	0.37% (1.52 ppm)	0.59% (2.44 ppm)
Single Slope with Baseline	0.40% (1.63 ppm)	0.35% (1.44 ppm)	0.75% (3.07 ppm)
Rolling Averages (2 slopes)	0.430% (1.76 ppm)	0.44% (1.80 ppm)	0.78% (3.20 ppm)
Rolling Averages (3 slopes)	0.441% (1.81 ppm)	-	0.75% (3.09 ppm)
Rolling Averages (4 slopes)	0.443% (1.82 ppm)	-	0.72% (2.94 ppm)
Rolling Averages (5 slopes)	0.447% (1.83 ppm)	-	0.65% (2.68 ppm)

This article is protected by copyright. All rights reserved.

Table 1. Methodological uncertainties (1σ) associated with each slope application method

Author Manuscript

This article is protected by copyright. All rights reserved.

Author Manuscript

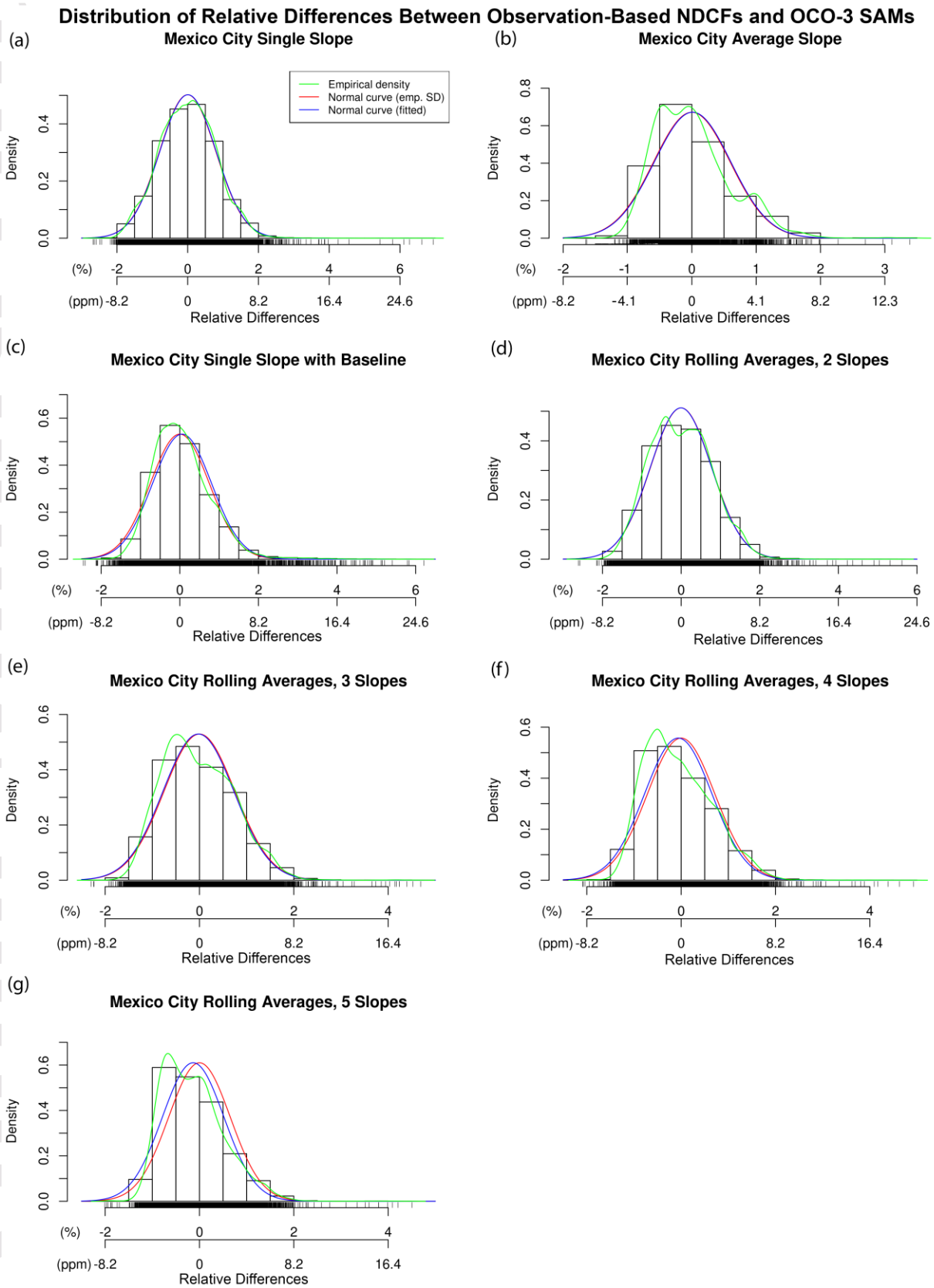


Figure 6. Same subplots as Figure 4, but for Mexico City, generated with 12 sets of

This article is protected by copyright. All rights reserved.

observations.

3.2 Methodological Uncertainties

3.2.1 Methodological Uncertainties in Observation-based NDCFs

Distributions of the relative differences between observation-based NDCFs and their corresponding SAMs, for each slope application method, are shown in Figures 4-6, with each figure corresponding to a different city. The standard deviations of these relative differences (listed in Table 1) represent the methodological uncertainties corresponding to their respective slope application methods and cities. Assuming 410 ppm as the concentration for a grid cell for illustrative purposes, these result in uncertainties ranging between about 1.4 and 3.3 ppm.

For Buenos Aires and Mexico City (Figures 4 and 6), as expected, we see that uncertainties are highest for the Single Slope method (panel (a) in both figures). Averaging with a baseline (c) or averaging all available slopes together (b) reduces uncertainties by dampening noise associated with the use of slopes that may be less representative. For Mexico City (Figure 6), we also observe the expected behavior: uncertainties are reduced as more slopes are averaged together (Figure 6d-g). For Buenos Aires (Figure 4d-g), we see the opposite behavior, though the uncertainties are fairly close to each other for these four cases of rolling averages. It appears that the particular slopes that are available for Buenos Aires generate greater relative differences when rolling averages are taken; we discuss this further regarding the mass balance estimates in Section 3.3.1. As for Melbourne (Figure 5), which has fewer co-located observations to derive slopes from, there are a few things of note. First, likely due to the limited number of observations, we see higher bias than for the other cities. Second, the Single Slope case (Figure 5a) demonstrates higher uncertainties than the cases involving the application of Average Slopes and Single Slope with Baseline (Figures 5b and c, respectively). Third, while the Single Slope (Figure 5a) and Rolling Averages of two slopes (Figure 5d) cases show very similar uncertainties, the latter actually has slightly higher uncertainty. We expect that this is also a peculiarity of the low number of observations used. However, the uncertainties are generally lower for Melbourne than the other cities, as a result of fairly similar slopes used.

3.2.2 Seasonality of Methodological Uncertainties

While the number of available SAMs limits our ability to assess seasonal effects in our results, we can assess the relative importance of seasonality in our observation-based results by interrogating the seasonality of the GEOS-CF simulation uncertainties, as the simulations are generated with the inclusion of biospheric activity and chemical effects like NO_2 photolysis. Figure 7 shows the spread of the simulated relative differences for all cities and seasons. With this figure, we assess the impact of seasonal effects on our method. The NDCF method involves generating total CO_2, which empirically captures seasonal effects in the slopes used. In Figure 7, we can see that the uncertainties for Buenos Aires, which experiences less biogenic variation during the year than the other two cities, do not demonstrate a seasonal pattern. The other two cities, Melbourne and Mexico City, do demonstrate some seasonality in their uncertainties, with lowest uncertainties in winter and highest in the summer. Accordingly, biospheric and chemical activity may have an impact on the uncertainties. However, while some variation across seasons could be attributed to seasonal differences in biological or chemical effects, the overall magnitude of the simulated uncertainties are dwarfed by the observational uncertainties discussed in 3.2.1. The simulation-based uncertainties range between 0.11 and 0.97 ppm if we

This article is protected by copyright. All rights reserved.

Author Manuscript

assume a concentration of 410 ppm, as compared to the 1.4 to 3.3 ppm that comprise the observational uncertainties. This suggests that, while we expect that seasonality may affect our results, the uncertainties associated with the observations that are absent from the simulations, such as observational noise and overpass time offsets between TROPOMI and OCO-3, are more significant sources of error. Thus, these seasonal effects do not appear to be the dominating source of error.

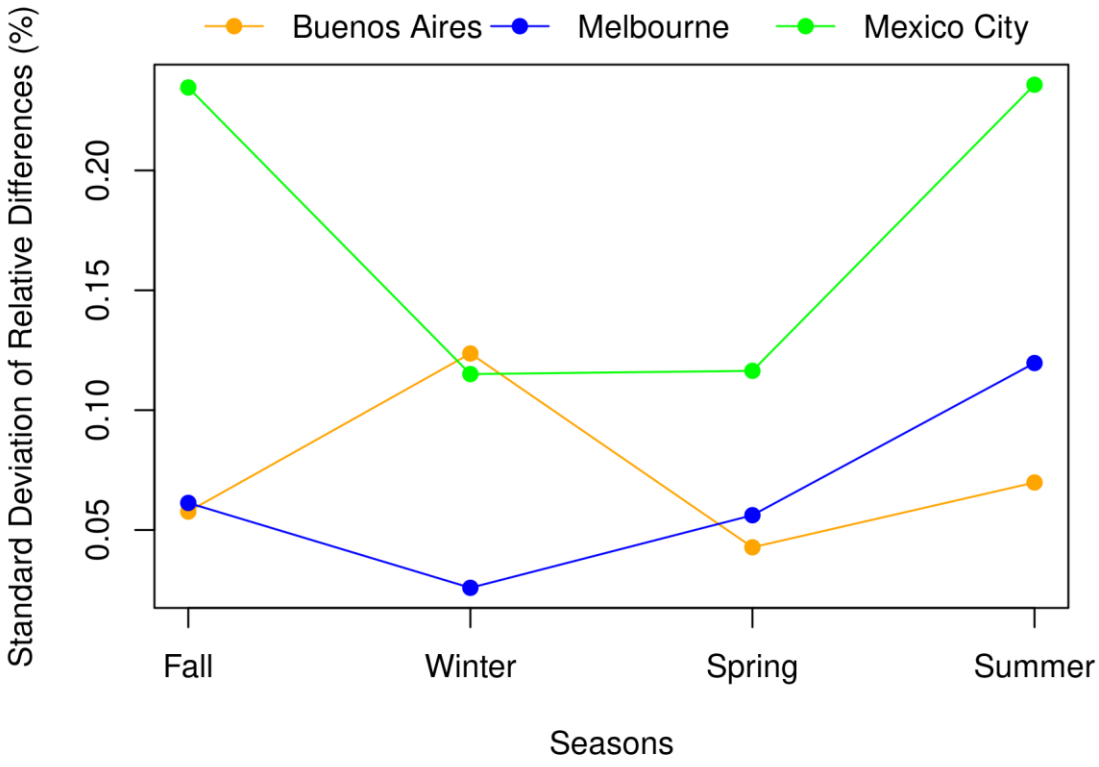


Figure 7. A seasonal comparison of the simulation uncertainties, where each season is determined by hemisphere. Note that these are for the time period of April 2019 to February 2020, so Mexico City's values have been reordered to follow the seasonal pattern of the other cities as opposed to their temporal order (e.g., fall is April 2019 for cities in the Southern Hemisphere and October 2019 for Mexico City). While there appear to be some seasonal (biospheric and chemical) effects on the Melbourne and Mexico City's uncertainties, the simulation uncertainties are small compared to the observational uncertainties. Accordingly, we expect seasonality may have an effect on the methodological uncertainties for both the simulations and observations but not act as the dominant source of error.

This article is protected by copyright. All rights reserved.

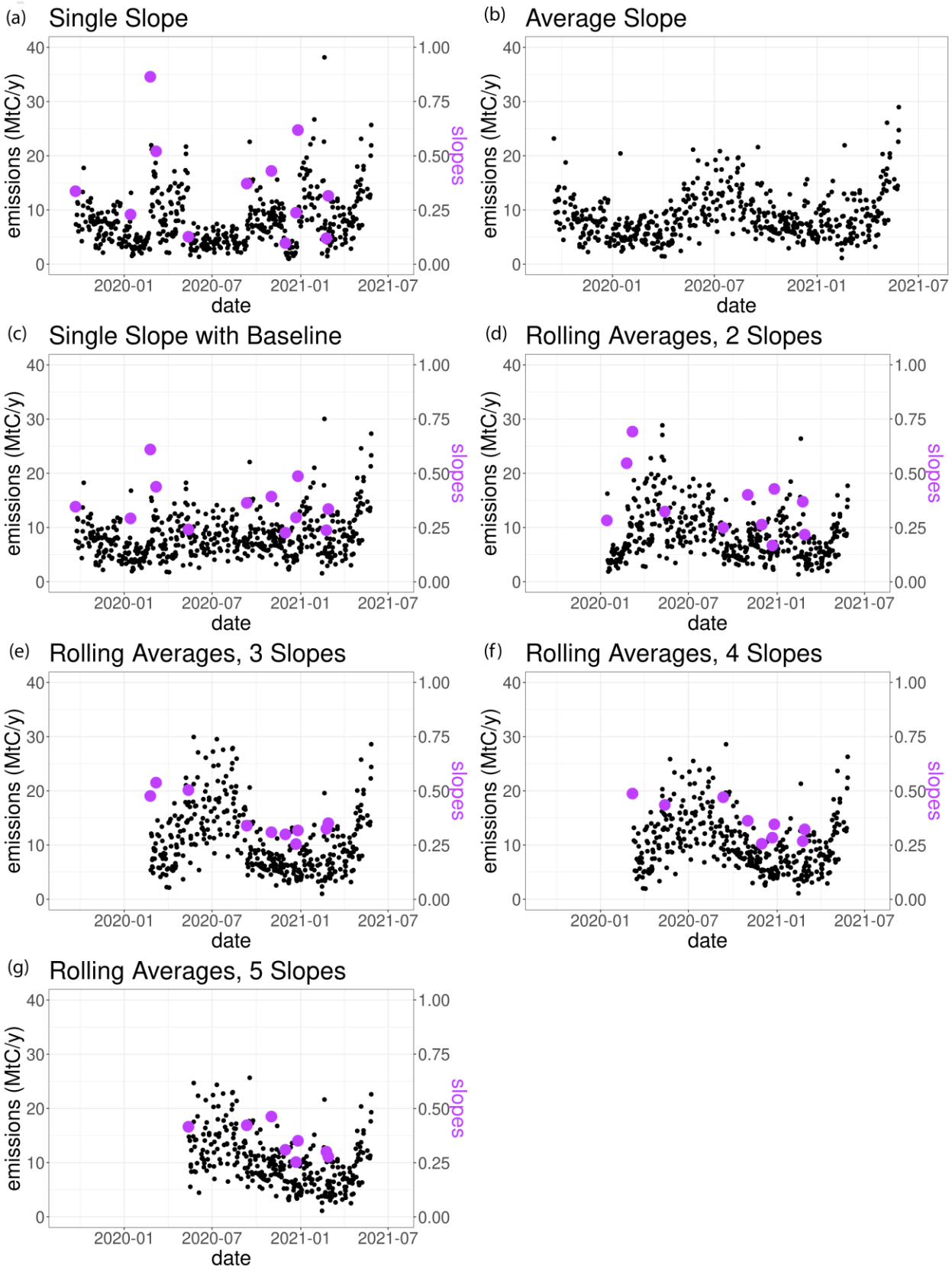
Author Manuscript

3.3 Emissions Estimates from Observation-based NDCFs

3.3.1 Emissions Estimates from NDCFs Generated from Remaining Available TROPOMI NO_2 Fields

We calculate mass balance estimates of NDCFs generated from all available TROPOMI NO_2 swaths, excluding those that are used in the co-located analysis and slope calculation, and plot time series of these estimates in Figures 8 (Buenos Aires) and S2-S3 (Melbourne and Mexico City). For each city, there are variations in the emissions estimates in time, especially depending on the value of the slopes used. This is particularly apparent for the Single Slope method for all three cities (e.g., Figure 8a). High or low slopes that are not representative and that are not averaged with any other values result in large periods of time with enhanced or suppressed emissions estimates that do not appear reasonable. This issue is potentially compounded with the Rolling Averages method if multiples of these types of slopes occur consecutively, which possibly explains the increased uncertainties for Buenos Aires with the Rolling Averages method discussed in Section 3.2.1. Despite these variations across methods, we observe that many of the time series suggest a seasonal cycle, with higher emissions in the winter than in the summer. Note that, while a seasonal cycle in emissions is reasonable in the context of these cities, the magnitude of the seasonal variations as seen in these plots may not fully account for differences between seasons in chemical and biological activity. The subannual variations we observe in the time series are more common in cases not using the Single Slope method. These other methods, which average more than one slope together, demonstrate more physically reasonable temporal variation. In particular, the Single Slope with Baseline method captures some of the temporality of the Single Slope method but dampens some of the noise from slopes that may not be representative of the entire period to which those slopes are applied. The Rolling Averages methods show relatively similar results for each city across the differing numbers of slopes used to generate the NDCFs. However, since the Rolling Averages method applies averaged slopes to NO_2 fields following the date of the latest slope used in the average, there is a greater loss of NO_2 data to be used to generate NDCFs with a greater number of slopes averaged.

This article is protected by copyright. All rights reserved.



This article is protected by copyright. All rights reserved.

Figure 8. Time series of mass balance estimates of Buenos Aires CO_2, calculated from NDCFs derived from the different slope application methods: (a) Single Slope, (b) Average Slope, (c) Single Slope with Baseline, (d) Rolling Averages (two slopes), (e) Rolling Averages (three slopes), (f) Rolling Averages (four slopes), and (g) Rolling Averages (five slopes). For all subplots other than (b), we show the slope used to generate all subsequent NDCFs in purple.

3.3.2 Emissions Estimates Aggregated Over Time

While uncertainties for individual NDCF emissions estimates are large, the value of the NDCF method becomes apparent in aggregate. Figures 9-11 show monthly averages of the mass balance estimates, with methodological uncertainties (excluding mass balance method uncertainties). These figures show all of the slope application methods together, along with the 2015 EDGAR monthly sectoral emissions estimates (with monthly values repeated across multiple years). In these figures, the monthly variations of the emissions estimates are quite apparent. These variations are in line with what is reported by EDGAR. Such monthly-scale estimates and variations have not previously been demonstrated by satellite estimates of CO_2 emissions. With the very large number of NO_2 swaths available for the generation of NDCFs, we can reduce uncertainty substantially in aggregate and capture unprecedented monthly emissions estimates.

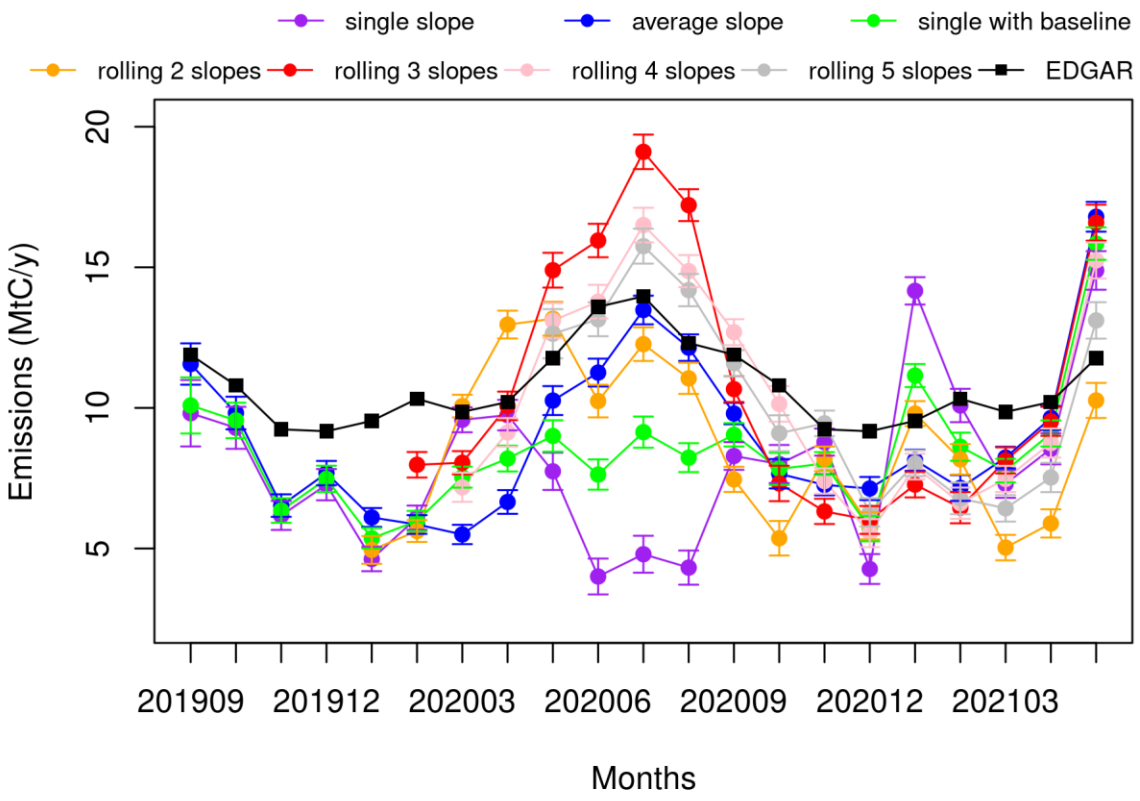


Figure 9. Mass balance estimates of Buenos Aires CO_2 averaged by month, with propagated uncertainties, corresponding to the different slope application methods in different colors (see legend). EDGAR monthly data for the year 2015 are shown in black squares, with multiples of

This article is protected by copyright. All rights reserved.

the same month showing repeated values. Each of these EDGAR points represents the sum of emissions from the four sectors of interest: power industry, manufacturing, road transport, and buildings.

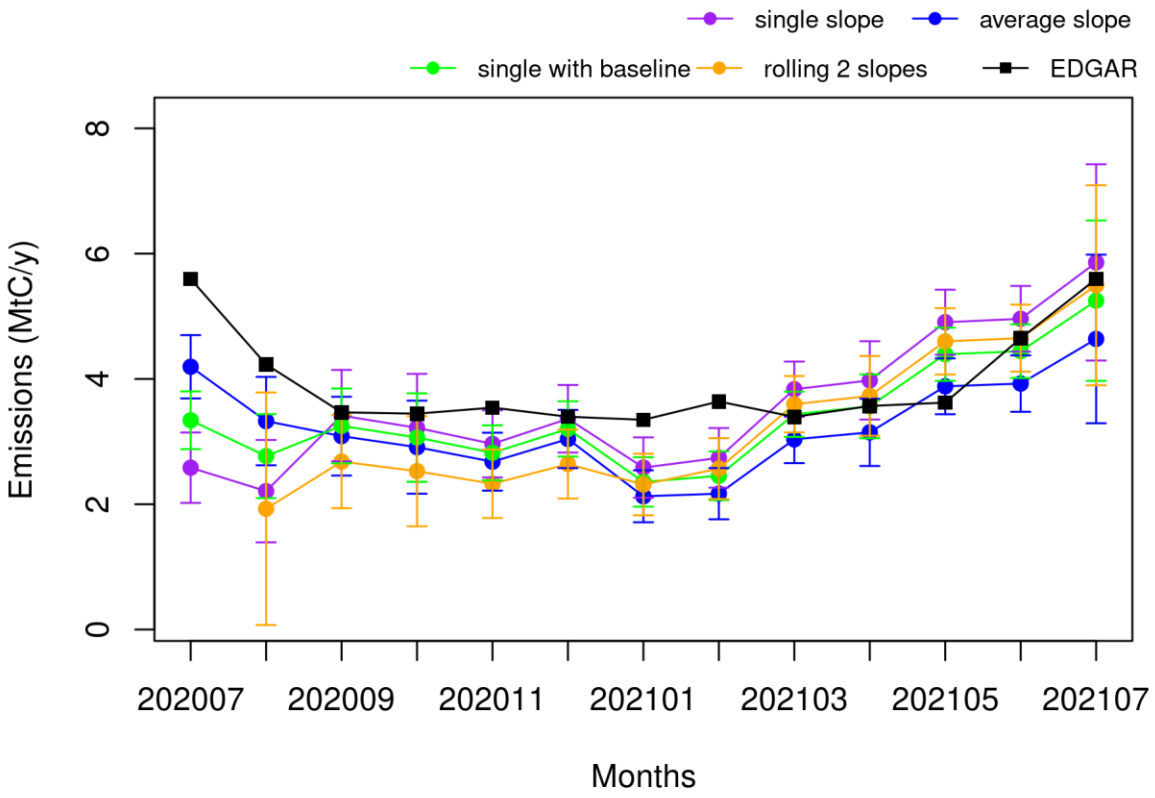


Figure 10. Same as Figure 9 but for Melbourne. Note that the low number of SAM observations limits the Rolling Averages method to two slopes only.

Author Manuscript

This article is protected by copyright. All rights reserved.

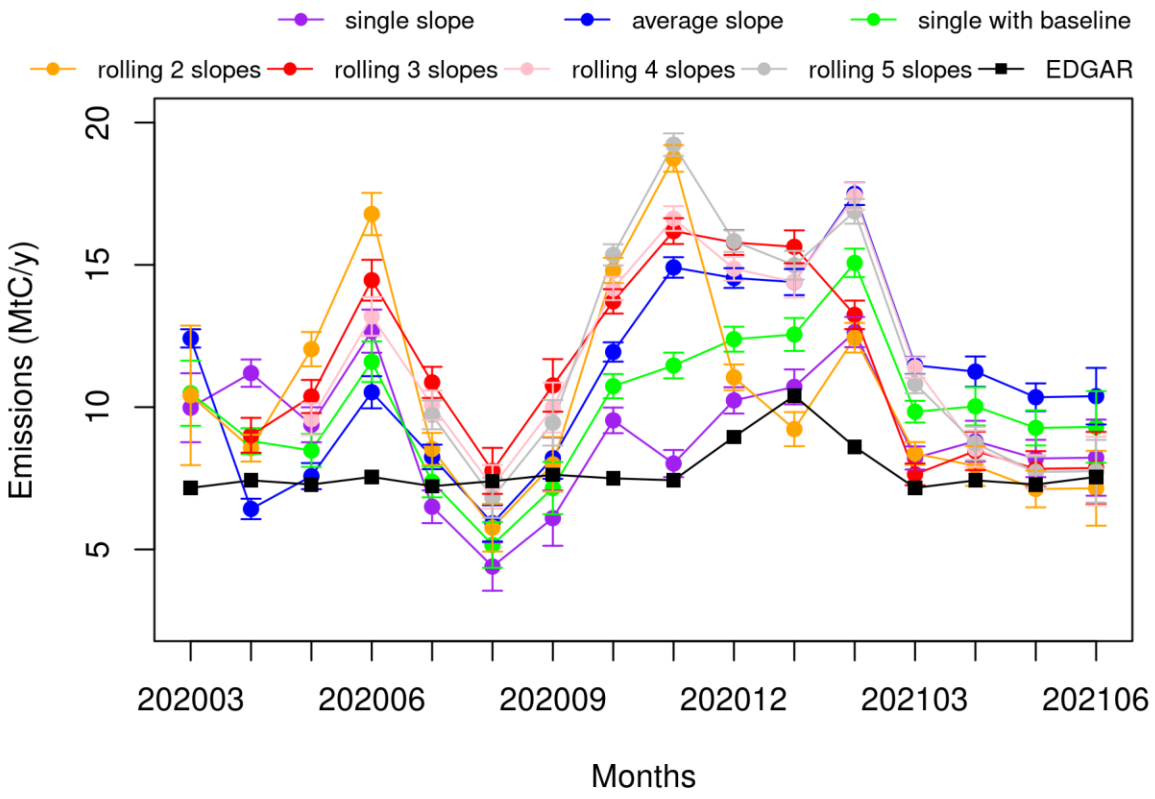


Figure 11. Same as Figure 9, but for Mexico City.

	Buenos Aires	*Melbourne*	*Mexico City*
Single Slope	7.82 ± 0.12	3.37 ± 0.18	9.33 ± 0.15
Average Slopes	8.63 ± 0.10	2.97 ± 0.12	11.70 ± 0.10
Single Slope with Baseline	8.21 ± 0.10	3.21 ± 0.14	10.35 ± 0.14
Rolling Averages (2 slopes)	8.52 ± 0.12	3.09 ± 0.19	10.98 ± 0.15
Rolling Averages (3 slopes)	10.49 ± 0.13	-	11.67 ± 0.15
Rolling Averages (4 slopes)	10.18 ± 0.14	-	12.31 ± 0.15
Rolling Averages (5 slopes)	9.97 ± 0.15	-	12.83 ± 0.14
EDGAR 2015	11.06	3.83	7.88

Table 2. Averaged emissions estimates in MtC y^{-1} across slope application methods and cities, with methodological uncertainties (1σ). EDGAR annual emissions estimates for the year 2015, for the four sectors addressed in this study, are also presented at the bottom.

This article is protected by copyright. All rights reserved.

Along with monthly estimates, we can average every mass balance estimate for a city and slope application method to estimate overall emissions over the time period of interest. Table 2 lists these estimates and their corresponding methodological uncertainties (excluding mass balance method uncertainties). Across methods, the emissions estimates are fairly similar to each other, with greater variation across methods with the inclusion of more unrepresentative slopes. As shown in the table, methodological uncertainties at this level of aggregation are quite low (ranging between about 1-6% of the estimates themselves), given the large number of NDCFs used in each of the averages. The much greater availability of TROPOMI swaths as opposed to SAMs demonstrates the utility of the NDCF method.

4 Discussion

Given the much greater availability of TROPOMI NO_2 data than OCO-3 SAM CO_2 data, the application of empirical relationships between CO_2 and NO_2 to the TROPOMI fields to generate NDCFs opens up many possibilities for assessing urban CO_2 emissions subannually and over time. Our study demonstrates monthly assessments of urban CO_2 emissions that have previously not been done before with satellite data.

Some CO_2-only studies have previously opted for wintertime data only to avoid influence from the biosphere (e.g., Wu et al., 2018), while NO_2 observation-based studies of CO_2 often used observations from only warm months due to the shorter NO_2 lifetime (e.g., Goldberg et al., 2019). As discussed in Section 3.2.2, we found that seasonality did have some effect on uncertainties, though uncertainties associated with observations such as observational noise and overpass time differences dominated the methodological uncertainties.. Accordingly, using the atmospheric correlation between NO_2 and CO_2 to generate NDCFs has the potential to provide a fairly simple method for estimating CO_2 emissions throughout the year, including during certain winter periods when satellite NO_2 observations can be made but CO_2 observations are not available due to greater sunlight needs. Future simulation-based studies, with increased granularity in the data so as to better parse out biological and chemical effects, would be valuable for interrogating the seasonality question further.

Single-day estimates of urban CO_2 emissions with the NDCF method would result in high methodological uncertainties, but aggregating emissions estimates from the large quantity of NDCFs that can be generated decreases uncertainties substantially. With the hundreds of NO_2 swaths taken over our study periods, our aggregated emissions estimates correspond to methodological uncertainties of only about 1-6% of the emissions estimates themselves (excluding uncertainties related to the mass balance method). Thus, we do not recommend the use of the NDCF method on a single-day basis but rather in aggregate, whether to assess subannual trends or to find an annual emissions estimate. Additionally, while a simple mass balance method is used in this study to demonstrate the utility of the NDCF method, methods that are more rigorous should be used in order to calculate more precise emissions estimates of CO_2 from NDCFs.

The NDCF method is shown to be a fairly powerful tool for assessment of time-averaged CO_2 emissions, though limited observational data of CO_2 may cause difficulties. In our study, we use a very limited number of SAMs (three) for Melbourne, due to limited overpasses and our data filtration. With only a small number of slopes to work with for this city, our mass balance emissions estimates are still reasonable as compared to EDGAR, as the slopes passing the filter

This article is protected by copyright. All rights reserved.

Author Manuscript

appear to be fairly representative. Filtering slopes is particularly important for a case like this, as a single unrepresentative slope could skew emissions estimates substantially.

Of the four slope application methods we explore in this study, we find that the Single Slope case is the most susceptible to physically unrealistic temporal fluctuations, whereas the other three result in more reasonable temporality in emissions estimates. While the Single Slope case is a near-real-time method for NDCF generation, we find that using this method relies on potentially noisy slopes that are not necessarily representative of the following days. The Average Slopes and Rolling Averages cases demonstrate monthly variations in emissions that we expect based on EDGAR (see Figures 9-11) and are much better candidates for use in future studies. For Buenos Aires and Mexico City, which have noisier slopes than Melbourne, the effect from this noise appears to have less of an impact with at least three slopes averaged in the Rolling Averages case (Figures 8 and S3), whereas the more uniform nature of the slopes used for Melbourne suggests that two slopes seem sufficient (Figure S2). Accordingly, future studies on other cities would likely need at least three slopes, though two could be appropriate in cities with low noise in slopes. The Single Slope with Baseline case captures temporal variations for Melbourne and Mexico City, but this is not demonstrated as much for Buenos Aires (Figures 8-11, S2-S3). This particular case seems to capture the temporality of slopes while dampening some of the potential noise associated with these slopes. Limited co-located observational data hampers our ability to understand how slopes change over time and evaluate how well the Single Slope and Single Slope with Baseline methods work. If higher frequencies of co-located observations were to be available, this would likely increase the utility of the Single Slope and Single Slope with Baseline methods, though with a high enough frequency it would be more sensible to use the CO_2 observations themselves rather than the NDCF method. Given the current state of data availability and the results of this study, using a slope application method that averages at least two slopes together seems to work well in aggregate. Overall, the use of the vast quantities of available NO_2 data to generate NDCFs and facilitate the study of urban CO_2 emissions is quite powerful.

This study focuses on three cities to demonstrate the feasibility of the NDCF method, with the cities being chosen largely due to limited SAM data availability at the time of the beginning of our study. This case study of three cities suggests that the NDCF method is promising, and additional SAM observations over time will allow for further exploration of the method to assess its more widespread applicability to cities not included in this study, such as large cities in Europe or North America outside of Mexico City. Additionally, the collection of more observations of both gases from future satellite missions such as Global Observing SATellite for Greenhouse gases and Water cycle (GOSAT-GW) and Copernicus CO2 Monitoring Mission (CO2M), which will observe these gases concurrently, will greatly improve our ability to use the NDCF method by increasing the available observations as well as by removing the challenges associated with having to use two different instruments. Until then, existing instruments like OCO-2 and OCO-3, as well as TROPOMI, will continue to play an important role in the evaluation of urban emissions.

5 Summary and Conclusions

Using proxy species such as NO_2 has proven to be a useful tool for the estimation of urban CO_2 emissions. In this study, we demonstrate a method of utilizing empirical relationships between satellite observations of CO_2 and NO_2 and applying these relationships to NO_2 fields to

This article is protected by copyright. All rights reserved.

Author Manuscript

generate NO_2-derived CO_2 fields, or NDCFs. We first establish this method with GEOS-CF simulations of these gases for the cities of Buenos Aires, Melbourne, and Mexico City, and then we evaluate the utility of the method on observations of CO_2 from OCO-3 in SAM mode and NO_2 from TROPOMI. We find methodological uncertainties from the standard deviation of relative differences at the grid cell level between the NDCFs and SAMs ranging between 0.35% (1.44 ppm assuming a 410 ppm concentration) and 0.79% (3.26 ppm). We also use a simple mass balance method to estimate emissions from NDCFs generated using four different slope application methods: Single Slope, Average Slopes, Single Slope with Baseline, and Rolling Averages. Slope application methods that average more than one slope together are more effective. We make monthly-scale emissions estimates that are comparable to monthly sectoral EDGAR emissions inventory estimates from 2015, an unprecedented temporal frequency achieved by space-based urban CO_2 emissions estimates. We also find that, due to the large number of TROPOMI NO_2 swaths available for the generation of NDCFs, our methodological uncertainties are drastically reduced when the emissions estimates are aggregated by month or longer. While the current availability of CO_2 satellite data limits the amount of information we can extract from such data on its own, the use of this data in conjunction with more abundant proxy data creates many possibilities for future studies to better understand and constrain urban CO_2 emissions.

Acknowledgments

Funding for this study was provided by the National Aeronautics and Space Administration (NASA) grants (80NSSC19K0092, 80NSSC21K1066, and 80NSSC21K1065) and the National Science Foundation Graduate Research Fellowship Grant No. DGE 1256260. The authors thank the OCO science team for general feedback and assistance with data acquisition.

Open Research

ODIAC2019 inventory data used for determining domains of interest in the study are available through the Center for Global Environmental Research, National Institute for Environmental Studies, Japan via http://doi.org/10.17595/20170411.001. GEOS-CF NO_2 simulation data used for establishing the NDCF method are available from the National Aeronautics and Space Administration (NASA) Goddard Space Flight Center Global Modeling and Assimilation Office (GMAO) via https://gmao.gsfc.nasa.gov/weather_prediction/GEOS-CF/data_access/ and Google Earth Engine (https://developers.google.com/earth-engine/datasets/catalog/NASA_GEOS-

This article is protected by copyright. All rights reserved.

Author Manuscript

CF_v1_rpl_tavg1hr, https://doi.org/10.1029/2020MS002413). OCO-3 Level 2 Lite, version 10.4r CO_2 observational data and TROPOMI Level 2 version 1 NO_2 observational data used for demonstrating the method are available through Goddard Earth Sciences Data and Information Services Center (GES DISC) via https://doi.org/10.5067/970BCC4DHH24 and https://doi.org/10.5270/S5P-s4ljg54, respectively. ERA5 wind data used for wind speeds to make mass balance estimates are available through Copernicus Climate Change Service (C3S) Climate Data Store (CDS) via https://doi.org/10.24381/cds.adbb2d47. EDGARv5.0 CO_2 and NO_2 monthly inventory data for the year 2015 used for comparison to NDCF mass balance estimates are available through the EDGARv5.0 greenhouse gas and air pollution websites (https://edgar.jrc.ec.europa.eu/dataset_ghg50 and https://edgar.jrc.ec.europa.eu/dataset_ap50) via https://data.jrc.ec.europa.eu/dataset/488dc3de-f072-4810-ab83-47185158ce2a and https://data.jrc.ec.europa.eu/dataset/377801af-b094-4943-8fdc-f79a7c0c2d19, respectively.

References

Berezin, E. V., Konovalov, I. B., Ciais, P., Richter, A., Tao, S., Janssens-Maenhout, G., et al. (2013). Multiannual changes of CO_2 emissions in China: indirect estimates derived from satellite measurements of tropospheric NO_2 columns. *Atmospheric Chemistry and Physics*, *13*(18), 9415–9438. https://doi.org/10.5194/acp-13-9415-2013

Bodansky, D. (2016). The Paris Climate Change Agreement: A New Hope? *American Journal of International Law*, *110*(2), 288–319. https://doi.org/10.5305/amerjintelaw.110.2.0288

Buchwitz, M., Schneising, O., Reuter, M., Heymann, J., Krautwurst, S., Bovensmann, H., et al. (2017). Satellite-derived methane hotspot emission estimates using a fast data-driven method. *Atmospheric Chemistry and Physics*, *17*(9), 5751–5774. https://doi.org/10.5194/acp-17-5751-2017

Ciais, P., Dolman, A. J., Bombelli, A., Duren, R., Peregon, A., Rayner, P. J., et al. (2014). Current systematic carbon-cycle observations and the need for implementing a policy-relevant carbon observing system. *Biogeosciences*, *11*(13), 3547–3602. https://doi.org/10.5194/bg-11-3547-2014

Copernicus Sentinel-5P (2018). TROPOMI Level 2 Nitrogen Dioxide total column products, Version 01 [Dataset]. European Space Agency. https://doi.org/10.5270/S5P-s4ljg54

Crippa, M., Guizzardi, D., Muntean, M., Schaaf, E., Lo Vullo, E., Solazzo, E., et al. (2019). EDGAR v5.0 Greenhouse Gas Emissions [Dataset]. European Commission, Joint

This article is protected by copyright. All rights reserved.

Research Centre (JRC). https://data.europa.eu/89h/488dc3de-f072-4810-ab83-47185158ce2a

Crippa, M., Solazzo, E., Huang, G., Guizzardi, D., Koffi, E., Muntean, M., et al. (2020). High resolution temporal profiles in the Emissions Database for Global Atmospheric Research. *Scientific Data*, *7*(1), 121. https://doi.org/10.1038/s41597-020-0462-2

Eldering, A., Taylor, T. E., O'Dell, C. W., & Pavlick, R. (2019). The OCO-3 mission: measurement objectives and expected performance based on 1 year of simulated data. *Atmospheric Measurement Techniques*, *12*(4), 2341–2370. https://doi.org/10.5194/amt-12-2341-2019

Fujinawa, T., Kuze, A., Suto, H., Shiomi, K., Kanaya, Y., Kawashima, T., et al. (2021). First Concurrent Observations of NO2 and CO2 From Power Plant Plumes by Airborne Remote Sensing. *Geophysical Research Letters*, *48*(14), e2021GL092685. https://doi.org/10.1029/2021GL092685

Gately, C. K., & Hutyra, L. R. (2017). Large Uncertainties in Urban-Scale Carbon Emissions. *Journal of Geophysical Research: Atmospheres*, *122*(20), 2017JD027359. https://doi.org/10.1002/2017JD027359

GEOS-CF. (2022). Goddard Earth Observing System Composition Forecasts [Dataset]. NASA GMAO. https://gmao.gsfc.nasa.gov/weather_prediction/GEOS-CF/data_access/

Goldberg, D. L., Lu, Z., Oda, T., Lamsal, L. N., Liu, F., Griffin, D., et al. (2019). Exploiting OMI NO2 satellite observations to infer fossil-fuel CO2 emissions from U.S. megacities. *Science of The Total Environment*, *695*, 133805. https://doi.org/10.1016/j.scitotenv.2019.133805

Gurney, K. R., Romero-Lankao, P., Seto, K. C., Hutyra, L. R., Duren, R., Kennedy, C., et al. (2015). Climate change: Track urban emissions on a human scale. *Nature News*, *525*(7568), 179. https://doi.org/10.1038/525179a

Hakkarainen, J., Ialongo, I., & Tamminen, J. (2016). Direct space-based observations of anthropogenic CO2 emission areas from OCO-2. *Geophysical Research Letters*, 2016GL070885. https://doi.org/10.1002/2016GL070885

Hakkarainen, Janne, Szelag, M. E., Ialongo, I., Retscher, C., Oda, T., & Crisp, D. (2021). Analyzing nitrogen oxides to carbon dioxide emission ratios from space: A case study of Matimba Power Station in South Africa. *Atmospheric Environment: X*, 100110. https://doi.org/10.1016/j.aeaoa.2021.100110

Hedelius, J. K., Liu, J., Oda, T., Maksyutov, S., Roehl, C. M., Iraci, L. T., et al. (2018). Southern California megacity CO_2, CH_4, and CO flux estimates using ground- and space-based remote sensing and a Lagrangian model. *Atmospheric Chemistry and Physics*, *18*(22), 16271–16291. https://doi.org/10.5194/acp-18-16271-2018

Hersbach, H., Bell, B., Berrisford, P., Biavati, G., Horányi, A., Muñoz Sabater, J., et al. (2018). ERA5 hourly data on single levels from 1959 to present [Dataset]. Copernicus Climate Change Service (C3S) Climate Data Store (CDS). https://doi.org/10.24381/cds.adbb2d47

Hersbach, H., Bell, B., Berrisford, P., Hirahara, S., Horányi, A., Muñoz-Sabater, J., et al. (2020). The ERA5 global reanalysis. *Quarterly Journal of the Royal Meteorological Society*, *146*(730), 1999–2049. https://doi.org/10.1002/qj.3803

Huber, D. E., Steiner, A. L., & Kort, E. A. (2020). Daily Cropland Soil NOx Emissions Identified by TROPOMI and SMAP. *Geophysical Research Letters*, *47*(22), e2020GL089949. https://doi.org/10.1029/2020GL089949

This article is protected by copyright. All rights reserved.

Author Manuscript

Hutyra, L. R., Duren, R., Gurney, K. R., Grimm, N., Kort, E. A., Larson, E., & Shrestha, G. (2014). Urbanization and the carbon cycle: Current capabilities and research outlook from the natural sciences perspective. *Earth's Future*, *2*(10), 2014EF000255. https://doi.org/10.1002/2014EF000255

International Energy Agency. (2008). *World Energy Outlook 2008*. International Energy Agency.

Janssens-Maenhout, G., Crippa, M., Guizzardi, D., Dentener, F., Muntean, M., Pouliot, G., et al. (2015). HTAP_v2.2: a mosaic of regional and global emission grid maps for 2008 and 2010 to study hemispheric transport of air pollution. *Atmospheric Chemistry and Physics*, *15*(19), 11411–11432. https://doi.org/10.5194/acp-15-11411-2015

Keller, C. A., Knowland, K. E., Duncan, B. N., Liu, J., Anderson, D. C., Das, S., et al. (2021). Description of the NASA GEOS Composition Forecast Modeling System GEOS-CF v1.0. *Journal of Advances in Modeling Earth Systems*, *13*(4), e2020MS002413. https://doi.org/10.1029/2020MS002413

Kiel, M., Eldering, A., Roten, D. D., Lin, J. C., Feng, S., Lei, R., et al. (2021). Urban-focused satellite CO2 observations from the Orbiting Carbon Observatory-3: A first look at the Los Angeles megacity. *Remote Sensing of Environment*, *258*, 112314. https://doi.org/10.1016/j.rse.2021.112314

Konovalov, I. B., Berezin, E. V., Ciais, P., Broquet, G., Zhuravlev, R. V., & Janssens-Maenhout, G. (2016). Estimation of fossil-fuel CO_2 emissions using satellite measurements of "proxy" species. *Atmospheric Chemistry and Physics*, *16*(21), 13509–13540. https://doi.org/10.5194/acp-16-13509-2016

Kort, E. A., Frankenberg, C., Miller, C. E., & Oda, T. (2012). Space-based observations of megacity carbon dioxide. *Geophysical Research Letters*, *39*(17), L17806. https://doi.org/10.1029/2012GL052738

Kuhlmann, G., Broquet, G., Marshall, J., Clément, V., Löscher, A., Meijer, Y., & Brunner, D. (2019). Detectability of CO_2 emission plumes of cities and power plants with the Copernicus Anthropogenic CO_2 Monitoring (CO2M) mission. *Atmospheric Measurement Techniques*, *12*(12), 6695–6719. https://doi.org/10.5194/amt-12-6695-2019

Kuhlmann, G., Brunner, D., Broquet, G., & Meijer, Y. (2020). Quantifying CO_2 emissions of a city with the Copernicus Anthropogenic CO_2 Monitoring satellite mission. *Atmospheric Measurement Techniques*, *13*(12), 6733–6754. https://doi.org/10.5194/amt-13-6733-2020

Kuze, A., Nakamura, Y., Oda, T., Yoshida, J., Kikuchi, N., Kataoka, F., et al. (2022). Examining partial-column density retrieval of lower-tropospheric CO2 from GOSAT target observations over global megacities. *Remote Sensing of Environment*, *273*, 112966. https://doi.org/10.1016/j.rse.2022.112966

Lauvaux, T., Gurney, K. R., Miles, N. L., Davis, K. J., Richardson, S. J., Deng, A., et al. (2020). Policy-Relevant Assessment of Urban CO2 Emissions. *Environmental Science & Technology*. https://doi.org/10.1021/acs.est.0c00343

Lei, R., Feng, S., Danjou, A., Broquet, G., Wu, D., Lin, J. C., et al. (2021). Fossil fuel CO2 emissions over metropolitan areas from space: A multi-model analysis of OCO-2 data over Lahore, Pakistan. *Remote Sensing of Environment*, *264*, 112625. https://doi.org/10.1016/j.rse.2021.112625

Lei, R., Feng, S., Xu, Y., Tran, S., Ramonet, M., Grutter, M., et al. (2022). Reconciliation of asynchronous satellite-based NO2 and XCO2 enhancements with mesoscale modeling over two urban landscapes. *Remote Sensing of Environment*, *281*, 113241. https://doi.org/10.1016/j.rse.2022.113241

This article is protected by copyright. All rights reserved.

Author Manuscript

Lin, J. C., Mitchell, L., Crosman, E., Mendoza, D. L., Buchert, M., Bares, R., et al. (2018). CO2 and Carbon Emissions from Cities: Linkages to Air Quality, Socioeconomic Activity, and Stakeholders in the Salt Lake City Urban Area. *Bulletin of the American Meteorological Society*, *99*(11), 2325–2339. https://doi.org/10.1175/BAMS-D-17-0037.1

Liu, F., Duncan, B. N., Krotkov, N. A., Lamsal, L. N., Beirle, S., Griffin, D., et al. (2020). A methodology to constrain carbon dioxide emissions from coal-fired power plants using satellite observations of co-emitted nitrogen dioxide. *Atmospheric Chemistry and Physics*, *20*(1), 99–116. https://doi.org/10.5194/acp-20-99-2020

Mueller, K. L., Lauvaux, T., Gurney, K. R., Roest, G., Ghosh, S., Gourdji, S. M., et al. (2021). An emerging GHG estimation approach can help cities achieve their climate and sustainability goals. *Environmental Research Letters*, *16*(8), 084003. https://doi.org/10.1088/1748-9326/ac0f25

Nassar, R., Hill, T. G., McLinden, C. A., Wunch, D., Jones, D. B. A., & Crisp, D. (2017). Quantifying CO2 Emissions From Individual Power Plants From Space. *Geophysical Research Letters*, *44*(19), 2017GL074702. https://doi.org/10.1002/2017GL074702

OCO-2/OCO-3 Science Team, Chatterjee, A., Payne, V. (2022). OCO-3 Level 2 bias-corrected XCO2 and other select fields from the full-physics retrieval aggregated as daily files, Retrospective processing v10.4r [Dataset]. Goddard Earth Sciences Data and Information Services Center (GES DISC). https://doi.org/10.5067/970BCC4DHH24

Oda, T., & Maksyutov, S. (2015). ODIAC Fossil Fuel CO_2 Emissions Dataset (Version name: ODIAC2019) [Dataset]. Center for Global Environmental Research, National Institute for Environmental Studies. https://doi.org/10.17595/20170411.001

Oda, T., Maksyutov, S., & Andres, R. J. (2018). The Open-source Data Inventory for Anthropogenic CO_2, version 2016 (ODIAC2016): a global monthly fossil fuel CO_2 gridded emissions data product for tracer transport simulations and surface flux inversions. *Earth System Science Data*, *10*(1), 87–107. https://doi.org/10.5194/essd-10-87-2018

Park, C., Jeong, S., Park, H., Yun, J., & Liu, J. (2020). Evaluation of the Potential Use of Satellite-Derived XCO2 in Detecting CO2 Enhancement in Megacities with Limited Ground Observations: A Case Study in Seoul Using Orbiting Carbon Observatory-2. *Asia-Pacific Journal of Atmospheric Sciences*. https://doi.org/10.1007/s13143-020-00202-5

Park, H., Jeong, S., Park, H., Labzovskii, L. D., & Bowman, K. W. (2021). An assessment of emission characteristics of Northern Hemisphere cities using spaceborne observations of CO2, CO, and NO2. *Remote Sensing of Environment*, *254*, 112246. https://doi.org/10.1016/j.rse.2020.112246

Reuter, M., Buchwitz, M., Schneising, O., Krautwurst, S., O'Dell, C. W., Richter, A., et al. (2019). Towards monitoring localized CO_2 emissions from space: co-located regional CO_2 and NO_2 enhancements observed by the OCO-2 and S5P satellites. *Atmospheric Chemistry and Physics*, *19*(14), 9371–9383. https://doi.org/10.5194/acp-19-9371-2019

Rosenzweig, C., Solecki, W., Hammer, S. A., & Mehrotra, S. (2010). Cities lead the way in climate-change action. *Nature*, *467*(7318), 909–911. https://doi.org/10.1038/467909a

United Nations, Department of Economic and Social Affairs, Population Division. (2019). *World Urbanization Prospects: The 2018 Revision (ST/ESA/SER.A/420)*. New York: United Nations.

Author Manuscript

This article is protected by copyright. All rights reserved.

Veefkind, J. P., Aben, I., McMullan, K., Förster, H., de Vries, J., Otter, G., et al. (2012). TROPOMI on the ESA Sentinel-5 Precursor: A GMES mission for global observations of the atmospheric composition for climate, air quality and ozone layer applications. *Remote Sensing of Environment*, *120*, 70–83. https://doi.org/10.1016/j.rse.2011.09.027

Weir, B., Ott, L. E., Collatz, G. J., Kawa, S. R., Poulter, B., Chatterjee, A., et al. (2021). Bias-correcting carbon fluxes derived from land-surface satellite data for retrospective and near-real-time assimilation systems. *Atmospheric Chemistry and Physics*, *21*(12), 9609–9628. https://doi.org/10.5194/acp-21-9609-2021

Wu, D., Lin, J. C., Fasoli, B., Oda, T., Ye, X., Lauvaux, T., et al. (2018). A Lagrangian approach towards extracting signals of urban CO_2 emissions from satellite observations of atmospheric column CO_2 (XCO_2): X-Stochastic Time-Inverted Lagrangian Transport model ("X-STILT v1"). *Geoscientific Model Development*, *11*(12), 4843–4871. https://doi.org/10.5194/gmd-11-4843-2018

Wu, D., Lin, J. C., Oda, T., & Kort, E. A. (2020). Space-based quantification of per capita CO2 emissions from cities. *Environmental Research Letters*, *15*(3), 035004. https://doi.org/10.1088/1748-9326/ab68eb

Yang, E. G., Kort, E. A., Wu, D., Lin, J. C., Oda, T., Ye, X., & Lauvaux, T. (2020). Using Space-Based Observations and Lagrangian Modeling to Evaluate Urban Carbon Dioxide Emissions in the Middle East. *Journal of Geophysical Research: Atmospheres*, *125*(7), e2019JD031922. https://doi.org/10.1029/2019JD031922

Ye, X., Lauvaux, T., Kort, E. A., Oda, T., Feng, S., Lin, J. C., et al. (2020). Constraining Fossil Fuel CO2 Emissions From Urban Area Using OCO-2 Observations of Total Column CO2. *Journal of Geophysical Research: Atmospheres*, *125*(8), e2019JD030528. https://doi.org/10.1029/2019JD030528

Author Manuscript

This article is protected by copyright. All rights reserved.